World Scientific
www.worldscientific.com

Coupled Analysis of Structural–Acoustic Problems Using the Cell-Based Smoothed Three-Node Mindlin Plate Element

Z. X. Gong*,†, Y. B. Chai*,† and W. Li*,†,‡,§

*Department of Naval Architecture and Ocean Engineering
Huazhong University of Science and Technology
Wuhan City, Hubei Province, 430074, P. R. China

†Hubei Key Laboratory of Naval
Architecture & Ocean Engineering Hydrodynamics (HUST)
Wuhan City, Hubei Province, 430074, P. R. China

‡Collaborative Innovation Center for Advanced
Ship and Deep-Sea Exploration (CISSE)
Shanghai City, 200240, P. R. China
§hustliw@hust.edu.cn

The cell-based smoothed finite element method (CS-FEM) using the original three-node Mindlin plate element (MIN3) has recently established competitive advantages for analysis of solid mechanics problems. The three-node configuration of the MIN3 is achieved from the initial, complete quadratic deflection via 'continuous' shear edge constraints. In this paper, the proposed CS-FEM-MIN3 is firstly combined with the face-based smoothed finite element method (FS-FEM) to extend the range of application to analyze acoustic fluid–structure interaction problems. As both the CS-FEM and FS-FEM are based on the linear equations, the coupled method is only effective for linear problems. The cell-based smoothed operations are implemented over the two-dimensional (2D) structure domain discretized by triangular elements, while the face-based operations are implemented over the three-dimensional (3D) fluid domain discretized by tetrahedral elements. The gradient smoothing technique can properly soften the stiffness which is overly stiff in the standard FEM model. As a result, the solution accuracy of the coupled system can be significantly improved. Several superior properties of the coupled CS-FEM-MIN3/FS-FEM model are illustrated through a number of numerical examples.

Keywords: Smooth finite element method (S-FEM); three-node Mindlin plate element (MIN3); gradient smoothing technique; structural–acoustic; numerical method.

1. Introduction

Structural–acoustic problems have attracted widespread attention in different engineering applications that are closely related to our daily life. The focal and difficult point is how to handle with the interaction between the acoustic fluid and the

attached structure. Hence, it is very important and necessary to do the research on structural–acoustic system in various engineering situations. Until now, analytical methods have only developed for coupled system with simple settings. When it comes to practical engineering problems with complex geometrical shape, the analytical solutions is not available and the numerical methods are adopted to solve the coupled issues. Over the last few decades, various numerical methods have been used to deal with these coupled problems where both the structure and the fluid domains are taken into consideration. In general, the structure is formulated based on displacement while we can employ several variables, such as displacement [Zienkiewicz and Bettess (1978)], fluid pressure [He *et al.*, 2010a; 2010b; Nguyen-Thoi *et al.* (2013a); Li *et al.* (2014)], potential [Everstine (1981)] and combination of them [Bathe *et al.* (1995); Wang and Bathe (1997)], to formulate the fluid. In this study, we use acoustic pressure to describe fluid domain and displacement to describe the structure domain for coupled acoustic fluid–structure system, respectively.

The boundary element method (BEM) and the standard finite element method (FEM) are currently the most widely used and well-established numerical tools for acoustic problems [Citarella *et al.* (2007); Cheng *et al.* (2008, 2009); He *et al.* (2011); Mukherjee and Liu (2013)]. Several specific numerical methods have been briefly proposed, including the Galerkin/least-squares (GLS) FEMs [Harari and Hughes (1992); Thompson and Pinsky (1995)], the discontinuous enrichment method (DEM) [Alvarez *et al.* (2006); Loula *et al.* (2007)] and element-free Galerkin method (EFGM) [Bouillard and Suleaub (1998)], where our interest is not here. For acoustic problems, the results of FEM model usually deviate substantially from the exact solutions by reason of the overly stiff phenomenon [Liu and Quek (2003)]. To improve the shortcoming of standard FEM, Liu and his group proposed the node-based smoothed point interpolation method (NS-PIM) [Liu and Gu (2001)] and linearly conforming point interpolation method (LC-PIM) [Liu *et al.* (2005); Zhang *et al.* (2007)] by incorporating the generalized gradient smoothing technique [Liu (2008)] with meshfree method. Furthermore, the node-based smoothed finite element method (NS-FEM) has been developed on the base of NS-PIM which could soften the stiffness of FEM model. However, NS-FEM and NS-PIM cannot be applied in a straight way for dynamic problems as they are found to be temporally instable [Liu *et al.* (2009)].

To overcome the drawback of NS-FEM, a cell-based smoothed FEM (CS-FEM) [Liu *et al.* (2007a, 2007b)] for 2D domain and a face-based smoothed FEM (FS-FEM) [Nguyen-Thoi *et al.* (2009a, 2009b)] for 3D domain have been developed using different gradient smoothing operations. The smoothing domains of CS-FEM are located inside the triangular, while those of FS-FEM are associated with face of two adjacent tetrahedral elements. Through the smoothing operations, both the two smoothing methods have a very close-to-exact stiffness. Hence, the CS-FEM and FS-FEM are both not only spatially stable but also temporally stable, so that they are very appropriate to deal with coupled structural–acoustic dynamic problems.

During the past few decades, three-node triangular plate elements with linear deflection have been used frequently. To take advantage of simplicity and flexibility of triangular element and improve its accuracy, the original MIN3 element with quadratic deflection proposed by Tessler and Hughes [1985] is introduced. Recently, Nguyen-Thoi and his group have combined the CS-FEM with MIN3 (CS-FEM-MIN3) to formulate a cell-based smoothed three-node Mindlin plate element (CS-MIN3) to study dynamic response of plate and laminated composite plates [Nguyen-Thoi *et al.* (2013b); Luong-Van *et al.* (2014)]. The results from Ngugen-Thoi and Luong-Van show that the CS-FEM-MIN3 is immune from shear-locking problem and shows the competitiveness to some other smoothed methods. However, so far, the CS-FEM-MIN3 has not yet applied for acoustic problems, such as coupled vibro-acoustic problems.

This paper hence extends the range of usage of CS-MIN3 by incorporating the CS-FEM-MIN3 with FS-FEM to analyze the structural–acoustic systems. It is anticipated that the results obtained from CS-FEM-MIN3/FS-FEM will be more accurate than those of FEM/FEM. Also, the smoothed results will be closer to the exact solutions. A model coupling two-dimensional (2D) CS-FEM-MIN3 with three-dimensional (3D) FS-FEM is introduced to simulate the system of the flexible plate interacting with 3D acoustic cavity. The cell-based smoothed operations are implemented over the 2D structure domain discretized by triangular elements, while the face-based operations are implemented over the 3D fluid domain discretized by tetrahedral elements. In the interface between the fluid domain and the structural domain, the normal fluid velocity must be equal to the normal structural velocity. Based on the above, the coupled govern equation can be formulated and can be utilized to solve practical engineering problems with complicated geometries.

2. Structure Domain

2.1. *Kinematic equations of plate*

For the coupled structural–acoustic problems, the influence of the acoustic fluid on the thin and flexible structures cannot be neglected. Commonly, shell and plate elements are employed to model the thin-walled structure in numerical simulations. In my study, the formulation will comply with the first-order Reissner–Mindlin plate theory. Therefore, based on the assumptions of above theory, considering the Cartesian coordinate, the displacements can be written as

$$w = w_0(x, y), \quad u = -z\beta_y(x, y), \quad v = -z\beta_x(x, y), \tag{1}$$

where w_0 be the transverse deflection, β_x and β_y are the rotations of the normal to the middle surface of the plate around the y-axis and x-axis, respectively. Figure 1 shows the Reissner–Mindlin flat plate and positive directions of deflection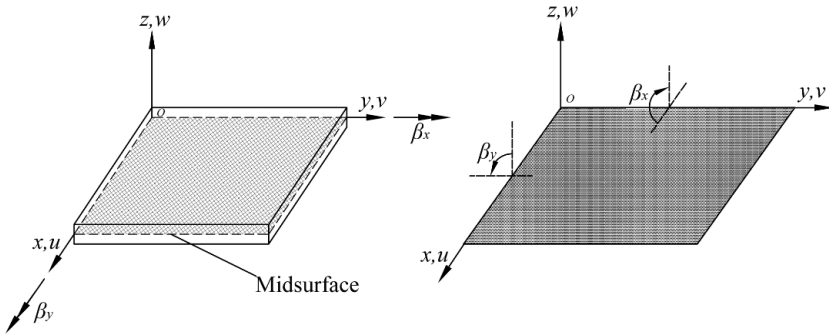 and two rotations. The curvature of the deflected plate $\boldsymbol{\kappa}$ and the shear strains $\boldsymbol{\gamma}$ can be

Fig. 1. The deflection w and two rotations β_x, β_y of Reissner–Mindlin flat plate in Cartesian coordinate system.

expressed as

$$\boldsymbol{\kappa}^T = \left[\frac{\partial \beta_x}{\partial x} \ \frac{\partial \beta_y}{\partial y} \ \frac{\partial \beta_x}{\partial y} + \frac{\partial \beta_y}{\partial x} \right], \quad \boldsymbol{\gamma} = \begin{bmatrix} \dfrac{\partial w}{\partial x} + \beta_x \\ \dfrac{\partial w}{\partial y} + \beta_y \end{bmatrix}. \tag{2}$$

By substituting the strains shown in Eq. (2) into the generalized smoothed Garlerkin (GS-Galerkin) weak form [Liu (2008)], we can obtain the govern equations for discretized system given by:

$$(\mathbf{K} - \omega^2 \mathbf{M})\{\mathbf{u}\} = \{\mathbf{F}\}, \tag{3}$$

where ω is the angular frequency:

$$\mathbf{K} = \int_{\Omega} \mathbf{B}^T \mathbf{D}_b \mathbf{B} d\Omega + \int_{\Omega} \mathbf{S}^T \mathbf{D}_s \mathbf{S} d\Omega \quad \text{(The stiffness matrix)}, \tag{4}$$

$$\mathbf{M} = \int_{\Omega} \rho \mathbf{N}_s^T \text{diag} \left[\frac{t^3}{12} \ \frac{t^3}{12} \ t \right] \mathbf{N}_s d\Omega \quad \text{(The mass matrix)}, \tag{5}$$

$$\mathbf{F} = \int_{\Gamma_s} \mathbf{N}_s^T \tau d\Gamma \quad \text{(The force vector)} \tag{6}$$

in which the $\mathbf{B}$ is the bending strain matrix, $\mathbf{S}$ is the shear strain matrix; $\mathbf{N}_s$ are the FEM shape functions and t denotes the thickness of the plate. The bending stiffness constitutive coefficients $\mathbf{D}_b$ and the transverse shear stiffness constitutive coefficients $\mathbf{D}_s$ are given as follows:

$$\mathbf{D}_b = \frac{Et^3}{12(1 - v^2)} \begin{bmatrix} 1 & v & 0 \\ v & 1 & 0 \\ 0 & 0 & (1-v)/2 \end{bmatrix}; \quad \mathbf{D}_s = ktG \begin{bmatrix} 1 & 0 \\ 0 & 1 \end{bmatrix}, \tag{7}$$

where G represents the shear modulus, $k = 5/6$ represents the shear correction factor, v and E are Poisson's and Young's ratio, respectively.

2.2. *The formulations of MIN3*

The main assumption of MIN3 is that at three field nodes, the two rotations of MIN3 are both linear, while the deflection is quadratic at six nodes in the original unconstrained MIN3 (three midpoints of three edges and three field nodes of the elements). Via continuous shear edge constraints, the deflection degrees of freedom (DOFs) at three midpoints of three edges can be removed as desired, and then the deflection can be obtained approximately only by vertex DOFs at three field nodes of the triangular elements. Numerical examples conducted by Tessler and Hugnes [1985] verified that the MIN3 element can overcome the shear-locking problems and also produces rapidly convergent solutions.

As shown in Fig. 2, using the three-node triangular element mesh, the two linear rotations β_x and β_y can be expressed as

$$\beta_x = \sum_{I=1}^{3} N_I(\mathbf{x})\beta_{xI} = \mathbf{N}\beta_x \quad \beta_y = \sum_{I=1}^{3} N_I(\mathbf{x})\beta_{yI} = \mathbf{N}\beta_y \tag{8}$$

and the initial quadratic deflection w can be expressed as

$$w = \sum_{I=1}^{6} R_I(\mathbf{x})w_I = \mathbf{R}\mathbf{w}_{ini}, \tag{9}$$

where $\mathbf{N} = [N_1(\mathbf{x}) \quad N_2(\mathbf{x}) \quad N_3(\mathbf{x})]$ denotes the row vector of linear shape functions at the corresponding nodes; $\boldsymbol{\beta}_x^T = [\beta_{x1} \quad \beta_{x2} \quad \beta_{x3}]$ and $\boldsymbol{\beta}_y^T = [\beta_{y1} \quad \beta_{y2} \quad \beta_{y3}]$ are the rotational DOFs at three nodes of the element; $\mathbf{w}_{ini}^T = [w_1 \quad w_2 \quad w_3 \quad w_4 \quad w_5 \quad w_6]$ is the unconstrained deflection DOFs at six nodes (shown in Table 1). $\mathbf{R}$ represents the associated vector of quadratic shape functions expressed as follows:

$$\mathbf{R} = [N_1(2N_1 - 1) \quad N_2(2N_2 - 1) \quad N_3(2N_3 - 1) \quad 4N_1N_2 \quad 4N_2N_3 \quad 4N_3N_1] \tag{10}$$
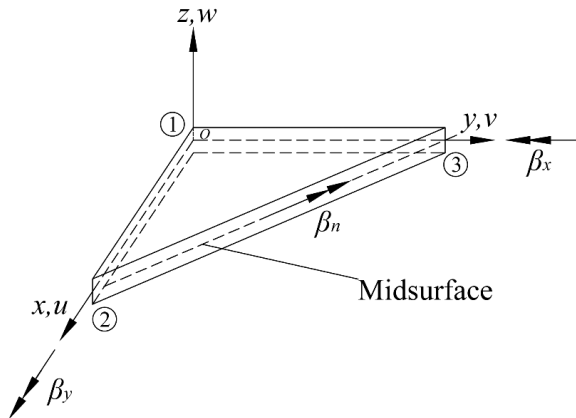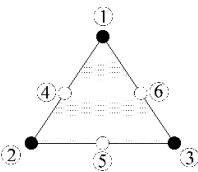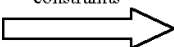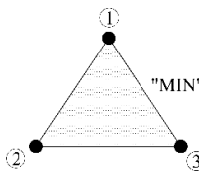
Fig. 2. Three-node triangular element.

Table 1. The forming process of MIN3 element.

Shape functions		Unconstrained nodal configuration	Differential relation: $(w,_s + \beta_n),_s\|_{\text{edges}} = 0$	Constrained nodal configuration
w	β_x, β_y			
Quadratic	Linear		Three edge constraints	"MIN"

Equations (8) and (9) can formulate the element matrices directly. However, to make the nodes of MIN3 simple, it is advantageous to remove the deflection DOFs at three midpoints of three edges, that is, w_4, w_5, w_6 in w. This can be achieved by enforced continuous shear edge constraints at each edge of MIN3 in the following differential relation

$$(w,_s + \beta_n),_s|_{\text{edges}} = 0, \tag{11}$$

where β_n denotes the tangential edge rotation and s is used to describe the edge coordinate, as shown in Fig. 2. The constraints enforced by Eq. (11) at the three element edges can generate the following formulations as

$$w_4 = \frac{1}{2}(w_1 + w_2) + \frac{1}{8}[b_3(\beta_{x1} - \beta_{x2}) + a_3(\beta_{y2} - \beta_{y1})],$$

$$w_5 = \frac{1}{2}(w_2 + w_3) + \frac{1}{8}[b_1(\beta_{x2} - \beta_{x3}) + a_1(\beta_{y3} - \beta_{y2})], \tag{12}$$

$$w_6 = \frac{1}{2}(w_3 + w_1) + \frac{1}{8}[b_2(\beta_{x3} - \beta_{x1}) + a_2(\beta_{y1} - \beta_{y3})],$$

where $a_1 = x_3 - x_2$, $b_1 = y_2 - y_3$, $a_2 = x_1 - x_3$, $b_2 = y_3 - y_1$, $a_3 = x_2 - x_1$, $b_3 = y_1 - y_2$, the relations between coordinates $(x_1, y_1, x_2, y_2, x_3, y_3)$ and coefficients $a_1, a_2, a_3, b_1, b_2, b_3$ are given by Fig. 3.

By substituting Eq. (12) into w in Eq. (9), the only constrained deflection field in terms of vertex DOFs is given by

$$w = \sum_{I=1}^{3} N_I w_I + \sum_{I=1}^{3} H_I \beta_{xI} + \sum_{I=1}^{3} L_I \beta_{yI}$$

$$= \mathbf{N}\mathbf{w} + \mathbf{H}\boldsymbol{\beta}_x + \mathbf{L}\boldsymbol{\beta}_y, \tag{13}$$

where $\mathbf{N} = [N_1 \ \ N_2 \ \ N_3], \mathbf{H} = [H_1 \ \ H_2 \ \ H_3], \mathbf{L} = [L_1 \ \ L_2 \ \ L_3]$ meet the requirements $\sum_{I=1}^{3} N_I \equiv 1$, $\sum_{I=1}^{3} H_I \equiv 0$, $\sum_{I=1}^{3} L_I \equiv 0$, respectively, to satisfy the fundamental constant strain criterion. Quadratic shape functions are formulated in
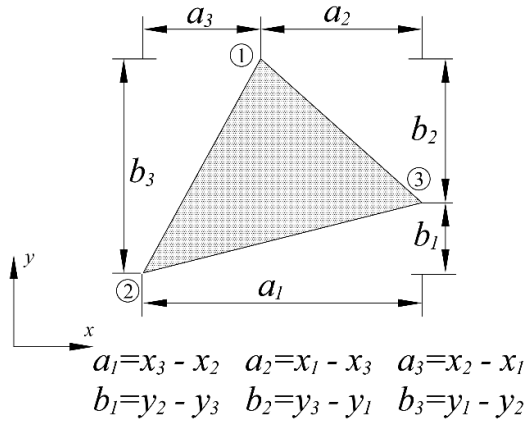
$$a_1 = x_3 - x_2 \quad a_2 = x_1 - x_3 \quad a_3 = x_2 - x_1$$
$$b_1 = y_2 - y_3 \quad b_2 = y_3 - y_1 \quad b_3 = y_1 - y_2$$

Fig. 3. The coordinate description in the MIN3.

the form of the linear shape functions as follows

$$H_1 = \frac{1}{2}(a_2 N_3 N_1 - a_3 N_1 N_2); \quad L_1 = \frac{1}{2}(b_3 N_1 N_2 - b_2 N_3 N_1),$$

$$H_2 = \frac{1}{2}(a_3 N_1 N_2 - a_1 N_2 N_3); \quad L_2 = \frac{1}{2}(b_1 N_2 N_3 - b_3 N_1 N_2), \tag{14}$$

$$H_3 = \frac{1}{2}(a_1 N_2 N_3 - a_2 N_3 N_1); \quad L_3 = \frac{1}{2}(b_2 N_3 N_1 - b_1 N_2 N_3).$$

Then the MIN3 element stiffness matrix can be given by

$$\mathbf{K}_e^{\mathrm{MIN3}} = \int_{\Omega_e} \mathbf{B}^T \mathbf{D}_b \mathbf{B} d\Omega + \int_{\Omega_e} \mathbf{S}^T \hat{\mathbf{D}}_{\mathbf{s}} \mathbf{S} d\Omega \tag{15}$$

where

$$\mathbf{B} = \begin{bmatrix} 0 & 0 & \mathbf{N}_{,x} \\ 0 & \mathbf{N}_{,y} & 0 \\ 0 & \mathbf{N}_{,x} & \mathbf{N}_{,y} \end{bmatrix}; \quad \mathbf{S} = \begin{bmatrix} \mathbf{N}_{,x} & \mathbf{L}_{,x} & \mathbf{H}_{,x} + \mathbf{N} \\ \mathbf{N}_{,y} & \mathbf{L}_{,y} + \mathbf{N} & \mathbf{H}_{,y} \end{bmatrix}. \tag{16}$$

To further improve the accuracy of solution, $\hat{\mathbf{D}}_s$ is introduced to replace $\mathbf{D}_s$ in Eq. (15) [Bischoff and Bletzinger (2001)]

$$\hat{\mathbf{D}}_s = \frac{Gkt^3}{t^2 + \alpha h_e^2} \begin{bmatrix} 1 & 0 \\ 0 & 1 \end{bmatrix} \tag{17}$$

in which α is a positive constant [Lyly *et al.* (1993)] and h_e is the longest length among three edges of the element.

2.3. *Formulation of CS-MIN3*

In the section, a new triangular element named a CS-MIN3 is established through the combination of cell-based strain smoothing technique and MIN3. The new triangular element can be applied for the 2D plate elements. In the CS-MIN3, we

consider the cell-based smoothing domains Ω_k $(k = 1, 2, \ldots, N)$ as the numerical integration domains, not the original domains in standard FEM, where N is the total number of smoothing domains for 2D domains. The smoothing domain Ω_k, located inside the triangle, consists of three sub-triangles $(\Delta_1, \Delta_2, \Delta_3)$ which are generated by connecting the three field nodes to the central point O (refer to Fig. 4).

In the present method, the strains in each sub-triangle are computed using MIN3 (Eq. (16)) as same as those in standard FEM. Then, the cell-based stain smoothing operation is applied over each smoothing domain. The smoothed bending strain $\tilde{\boldsymbol{\kappa}}_k$ and smoothed shear strain $\tilde{\boldsymbol{\gamma}}_k$ can be calculated by

$$\tilde{\boldsymbol{\kappa}}_k = \int_{\Omega_k} \mathbf{k}\Phi_k(\mathbf{x})d\Omega, \tag{18}$$

$$\tilde{\gamma}_k = \int_{\Omega_k} \gamma\Phi_k(\mathbf{x})d\Omega. \tag{19}$$

In this study, we adopt the following simplest form of the smoothing function given by

$$\Phi_k(\mathbf{x}) = \begin{cases} 1/A_k & \mathbf{x} \in \Omega_k \\ 0 & \mathbf{x} \notin \Omega_k \end{cases}, \tag{20}$$

where A_k is the area of the kth smoothing domain. By implementing the cell-based strain smoothing operation, $\tilde{\boldsymbol{\kappa}}_k$ and $\tilde{\gamma}_k$ of the smoothing domain Ω_k in Eqs. (18) and (19) are further expressed by

$$\tilde{\boldsymbol{\kappa}}_k = \frac{A_{k,1}\mathbf{k}^{k,1} + A_{k,2}\mathbf{k}^{k,2} + A_{k,3}\mathbf{k}^{k,3}}{A_k} \tag{21}$$

$$\tilde{\gamma}_k = \frac{A_{k,1}\boldsymbol{\gamma}^{k,1} + A_{k,2}\boldsymbol{\gamma}^{k,2} + A_{k,3}\boldsymbol{\gamma}^{k,3}}{A_k} \tag{22}$$

where $A_{k,1}$, $A_{k,2}$ and $A_{k,3}$ are the areas of three sub-domains in the kth smoothing domain, respectively, with the whole smoothing domain area $A_k = A_{k,1} + A_{k,2} + A_{k,3}$.

With the above formulations, the smoothed bending strain $\tilde{\boldsymbol{\kappa}}_k$ and the smoothed shear strain $\tilde{\boldsymbol{\gamma}}_k$ can be obtained in the forms of corresponding smoothing bending
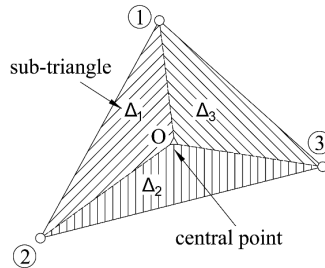

Fig. 4. The smoothing domain with three smoothing sub-domains located inside a triangular element.

strain matrix and shear strain matrix

$$\tilde{\boldsymbol{\kappa}}_k = \tilde{\mathbf{B}}_k \mathbf{d}_k, \quad \tilde{\gamma}_k = \tilde{\mathbf{S}}_k \mathbf{d}_k, \tag{23}$$

where $\mathbf{d}_k$ is vector of nodal DOFs of the smoothing domain, and

$$\tilde{\mathbf{B}}_k = \frac{A_{k,1}\mathbf{B}^{k,1} + A_{k,2}\mathbf{B}^{k,2} + A_{k,3}\mathbf{B}^{k,3}}{A_k} \quad \text{(The smoothed bending strain matrix)}, \tag{24}$$

$$\tilde{\mathbf{S}}_k = \frac{A_{k,1}\mathbf{S}^{k,1} + A_{k,2}\mathbf{S}^{k,2} + A_{k,3}\mathbf{S}^{k,3}}{A_k} \quad \text{(the smoothed shear strain matrix)}. \tag{25}$$

Substituting Eqs. (24) and (25) into Eq. (4), the smoothed element stiffness matrix can be expressed as

$$\tilde{\mathbf{K}}_k = \int_{\Omega_k} \tilde{\mathbf{B}}_k^T \mathbf{D}_b \tilde{\mathbf{B}}_k d\Omega + \int_{\Omega_k} \tilde{\mathbf{S}}_k^T \hat{\mathbf{D}}_s \tilde{\mathbf{S}}_k d\Omega = \tilde{\mathbf{B}}_k^T \mathbf{D}_b \tilde{\mathbf{B}}_k A_k + \tilde{\mathbf{S}}_k^T \hat{\mathbf{D}}_s \tilde{\mathbf{S}}_k A_k \tag{26}$$

Then the global stiffness matrix can be assembled using the following formulation

$$\tilde{\mathbf{K}} = \sum_{k=1}^{N} \tilde{\mathbf{K}}_k. \tag{27}$$

Note that the cell-base strain smoothing operation is implemented inside the triangular element, that is to say, the area of the smoothing domain equals that of the smoothed triangular element. Also, as shown in Eq. (23), the final formulations of strain matrices are only related to the nodal displacement vectors of three vertex nodes, without those of the central point. Hence, the central point is introduced for the smoothed operations and intermediate formulations without extra DOFs. Finally, with the same mesh, the form of stiffness matrix of CS-MIN3 coincides well with that in the MIN3.

3. 3D Fluid Domain

3.1. *Formulation for acoustic fluid domain*

Consider an acoustic fluid domain, let c denote the speed of sound traveling in the acoustic domain and p represents the field acoustic pressure. The wave equation in acoustic domain can be written as follows expressed:

$$\Delta p - \frac{1}{c^2}\frac{\partial^2 p}{\partial t^2} = 0, \quad \text{in } \Omega_f, \tag{28}$$

where and denote the Laplace operator and pc time, respectively.

The rigid boundary conditions in Ω_f of the acoustic cavity are given by the equation $\nabla p \cdot n = 0$, while at the structural–acoustic coupling interface Ω_{sf}, the boundary condition should turn to be $\nabla p \cdot n = -\rho \ddot{u}_f$. In the above equations, n represents the normal vector, $\boldsymbol{\rho}$ and $\ddot{u}_f$ are the mass density of fluid and the fluid normal acceleration component at the interaction face, respectively.

Through the gradient smoothing operations on the acoustic domain, the GS-Galerkin weak form can be formulated as

$$\frac{1}{c^2} \int_{\Omega_f} \delta p \cdot \frac{\partial^2 p}{\partial t^2} d\Omega_f - \int_{\Omega_f} \delta \widetilde{\nabla} p \cdot \widetilde{\nabla} p d\Omega_f + \rho \int_{\Omega_f} \delta p \cdot \ddot{u}_f d\Gamma = 0. \tag{29}$$

The finite element approximation of the acoustic pressure is interpolated using four nodal pressure of the element and can be described in terms of a set of shape functions as follows:

$$p = \sum_{i=1}^{n} \mathbf{N}_{fi} p_i = \mathbf{N}_f \mathbf{p}, \quad \delta p = \sum_{i=1}^{n} \mathbf{N}_{fi} \delta p_i = \mathbf{N}_f \delta \mathbf{p}, \tag{30}$$

where p_i and $\mathbf{N}_{fi}$ denote unknown pressure at the ith node and FEM shape function, respectively. By substituting Eq. (30) into the GS-Galerkin weak form given by Eq. (29), we can obtain the smoothed govern equation for the discretized system as following:

$$\mathbf{M}_f \{\ddot{\mathbf{p}}\} + \tilde{\mathbf{K}}_f \{\mathbf{P}\} = \{\mathbf{F}_f\}, \tag{31}$$

where

$$\mathbf{M}_f = \frac{1}{c^2} \int_{\Omega_f} \mathbf{N}_f^T \mathbf{N}_f d\Omega_f \quad \text{(The acoustic mass matrix)}, \tag{32}$$

$$\tilde{\mathbf{K}}_f = \int_{\Omega_f} \tilde{\mathbf{B}}_f^T \tilde{\mathbf{B}}_f d\Omega_f, \tag{33}$$

$$\mathbf{F}_f = -\rho \int_{\Omega_{sf}} \mathbf{N}_f^T \ddot{u}_f d\Gamma \quad \text{(The vector of nodal acoustic forces)}, \tag{34}$$

$$\{\mathbf{p}\}^T = \{p_1, p_2, \ldots, p_n\} \quad \text{(Nodal acoustic pressure in the domain)}. \tag{35}$$

3.2. *The FS-FEM for the acoustic fluid*

The FS-FEM has shown several superior properties in solving 3D solid mechanics problems, including 3D linear and geometrically nonlinear problems and visco-elastoplastic analyses [Nguyen-Thoi *et al.* (2009a, 2009b)]. It is anticipated that the FS-FEM will also perform very well for 3D acoustic problems. In FS-FEM, face-based smoothing operations are implemented over the smoothed domains which are formed on the base of the tetrahedral elements used in the standard FEM. As shown in Fig. 5, the smoothing domain Ω_k(BCDNM) is created by connecting the centroids of two adjacent tetrahedral elements (M and N) with three endpoints (B, C and D) of common face k.

The relation between the velocity v in acoustic domain and the gradient of acoustic pressure p can be given by

$$\nabla p = -j\rho\omega v. \tag{36}$$

In the FS-FEM acoustic model, the gradient smoothing technique is actually used to smooth the velocity field. By applying the divergence theorem, the smoothed
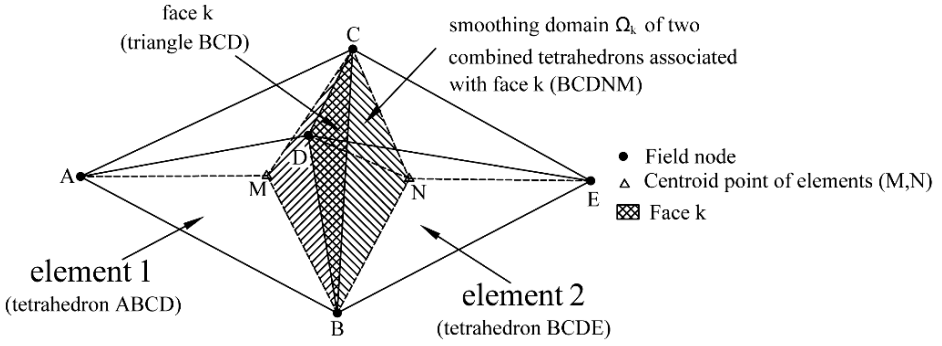
Fig. 5. The smoothing domain Ω_k (BCDNM) and two adjacent tetrahedral elements (ABCD, BCDE).

velocity $\tilde{v}(\mathbf{x}_k)$ is given by

$$\tilde{v}(\mathbf{x}_k) = \frac{1}{v_k} \int_{\Omega_k} v(\mathbf{x})d\Omega = -\frac{1}{j\rho\omega V_k} \int_{\Omega_k} \Delta p d\Omega = -\frac{1}{j\rho\omega V_k} \int_{\Gamma_k} p \cdot n d\Gamma, \quad (37)$$

where $V_k = \int_{\Omega_k} d\Omega$ represents the volume of smoothing domain for face k.

Substitute the field variable interpolated by a set of shape functions in Eq. (30) into Eq. (37), we can obtain the smoothed velocity as follows:

$$\tilde{v}(\mathbf{x}_k) = -\frac{1}{j\rho\omega} \sum_{i \in M_k} \tilde{\mathbf{B}}_{fi}(\mathbf{x}_k)p_i \quad (38)$$

where M_k is the total number of nodes in the smoothed domain associated with face k. The gradient-pressure matrix in 3D acoustic fluid is given by

$$\tilde{\mathbf{B}}_{fi}^T(\mathbf{x}_k = [\tilde{\mathbf{b}}_{i1} \quad \tilde{\mathbf{b}}_{i2} \quad \tilde{\mathbf{b}}_{i3}]), \quad (39)$$

$$\tilde{\mathbf{b}}_{ip} = \frac{1}{V_k} \int_{\Gamma_k} \mathbf{N}_{fi}(\mathbf{x})n_p(\mathbf{x})d\Gamma \quad (p = 1, 2, 3, \text{ for 3D problem}). \quad (40)$$

By using Gauss integration, provided that w_r denotes the weight of each Gauss point, N_s denoted the total number of boundary triangles of the smoothed domain Ω_k and N_g is the total number of Gauss points distributed for each surface triangle, the discretized form of Eq. (40) turns to be

$$\tilde{\mathbf{b}}_{ip} = \frac{1}{V_k} \sum_{q=1}^{N_s} \left[\sum_{r=1}^{N_g} w_r N_{fi}(\mathbf{x}_{qr})n_p(\mathbf{x}_q) \right]. \quad (41)$$

Then the smoothed stiffness matrix of smoothing domain Ω_k can be calculated as:

$$\tilde{\mathbf{K}}_f^{(k)} = \int_{\Omega_f} \tilde{\mathbf{B}}_f^T \tilde{\mathbf{B}}_f d\Omega_f = \tilde{\mathbf{B}}_f^T \tilde{\mathbf{B}}_f V_k \quad (42)$$

4. Coupling Formulations of Both Models

Based on the previous formulations of both the structure domain and the acoustic domain, the coupling formulations will be presented in this section. At the fluid–structure coupling interface, owing to the common motion shared by the fluid and the structure, two continuity conditions should be ensured, which the one is the continuity of the normal displacements in structure and the normal displacements in acoustic fluid, the other is the continuity between the acoustic fluid pressure and the structural stress. The interface boundary condition and the stress–pressure relations are respectively expressed as

$$u_s \mathbf{n} = u_f \mathbf{n}, \quad \text{on } \partial\Omega_{sf}, \tag{43}$$

$$\sigma_s|_n = -p, \quad \text{on } \partial\Omega_{sf}, \tag{44}$$

where u_s and u_f are the displacement of the structure and fluid at the interaction face, respectively.

According to the general principle of selecting the positive direction of normal, at the coupling interface, the normal on the plate $\mathbf{n}_s$ is opposite to the normal of fluid $\mathbf{n}_f$, which can be described by $\mathbf{n}_s = -\mathbf{n}_f$. The force loading of the acoustic pressure from the acoustic fluid on the attached plate can be written as follows:

$$\mathbf{F}_s = \int_{\partial\Omega_{sf}} \mathbf{N}_s^T \mathbf{n}_s \sigma_s d\Gamma = \int_{\partial\Omega_{sf}} \mathbf{N}_s^T \mathbf{n}_f p d\Gamma = \left(\int_{\partial\Omega_{sf}} \mathbf{N}_s^T \mathbf{n}_f \mathbf{N}_f d\Gamma \right) \mathbf{p}. \tag{45}$$

Similarly, the force loading of vibrating plate upon the acoustic domain can be also written in the following formulation:

$$\mathbf{F}_f = -\rho \int_{\partial\Omega_{sf}} \mathbf{N}_f^T \ddot{u}_f d\Gamma$$

$$= -\rho \int_{\partial\Omega_{sf}} \mathbf{N}_f^T \ddot{u}_s d\Gamma = -\rho \left(\int_{\partial\Omega_{sf}} \mathbf{N}_f^T \mathbf{n}_f \mathbf{N}_s d\Gamma \right) \ddot{\mathbf{u}}_s. \tag{46}$$

Now introducing the spatial coupling matrix

$$\mathbf{H} = \int_{\partial\Omega_{sf}} \mathbf{N}_s^T \mathbf{n}_f \mathbf{N}_f d\Gamma. \tag{47}$$

Substituting Eq. (47) into Eqs. (45) and (46), the components of coupling force are expressed in the following matrices:

$$\mathbf{F}_s = \mathbf{H}\mathbf{P}, \quad \mathbf{F}_f = -\rho\mathbf{H}^T \ddot{\mathbf{u}}_s. \tag{48}$$

Combining the structural CS-FEM model and acoustic FS-FEM model yields the govern equation for the coupled system. The formulation of the unsymmetrical

system can be written as

$$
\begin{bmatrix} \mathbf{M} & \mathbf{0} \\ \rho\mathbf{H}^T & \mathbf{M}_f \end{bmatrix} \begin{Bmatrix} \ddot{\mathbf{u}}_s \\ \ddot{\mathbf{p}} \end{Bmatrix} + \begin{bmatrix} \tilde{\mathbf{K}} & -\mathbf{H} \\ \mathbf{0} & \tilde{\mathbf{K}}_f \end{bmatrix} \begin{Bmatrix} \mathbf{u}_s \\ \mathbf{p} \end{Bmatrix} = \begin{Bmatrix} \mathbf{F}_s \\ \mathbf{F}_f \end{Bmatrix}.
\tag{49}
$$

Under harmonic forced excitations, the corresponding formulation from Eq. (49) is now given by:

$$
\left(\begin{bmatrix} \tilde{\mathbf{K}} & -\mathbf{H} \\ \mathbf{0} & \tilde{\mathbf{K}}_f \end{bmatrix} - \omega^2 \begin{bmatrix} \mathbf{M} & \mathbf{0} \\ \rho\mathbf{H}^T & \mathbf{M}_f \end{bmatrix} \right) \begin{Bmatrix} \mathbf{u}_s \\ \mathbf{p} \end{Bmatrix} = \begin{Bmatrix} \mathbf{F}_s \\ \mathbf{F}_f \end{Bmatrix}.
\tag{50}
$$

5. Typical Numerical Examples

To demonstrate the previous formulations of the combined CS-FEM-MIN3 (CS-MIN3) and FS-FEM described in the paper, several numerical examples are conducted in this section. The influence of mesh irregularity of plate is also evaluated both in standard FEM and smoothed FEM. The first part concerns a rectangular plate with two kinds of different boundary conditions for static analysis. The second part is a closed acoustic cavity with a flexible plate on top, including the free vibration analysis of the uncoupled and coupled system and the influence of nodal irregularity to system. The third part aims to illustrate the effectiveness and superiority of the above method for forced vibration analysis of a 3D tube filled with air with a flexible plate at the end.

5.1. *Static analysis of rectangular plate*

For static analysis, a rectangular plate with clamped and simply supported boundary conditions is studied respectively as shown in Figs. 6(a) and 6(b). The plate is subjected to a unit uniform load $q = 1$. The deflection at the center point of the plate is computed. The plate is made of aluminum with $\rho = 2{,}700\,\text{kg/m}^3, \mu = 0.3$ and $E = 71\,\text{Gpa}$, which has the dimension of $0.44\,\text{m} \times 0.38\,\text{m}$ with a thickness of $0.001\,\text{m}$. To evaluate the convergence of central deflection, the plate is discretized
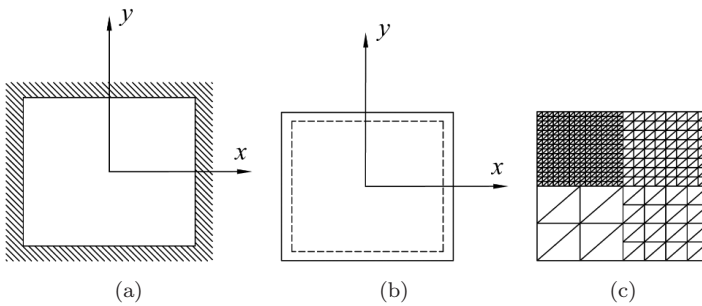

Fig. 6. Rectangular plate models with (a) clamped, (b) simply supported boundary conditions and (c) different triangular meshes of a quarter of plate.
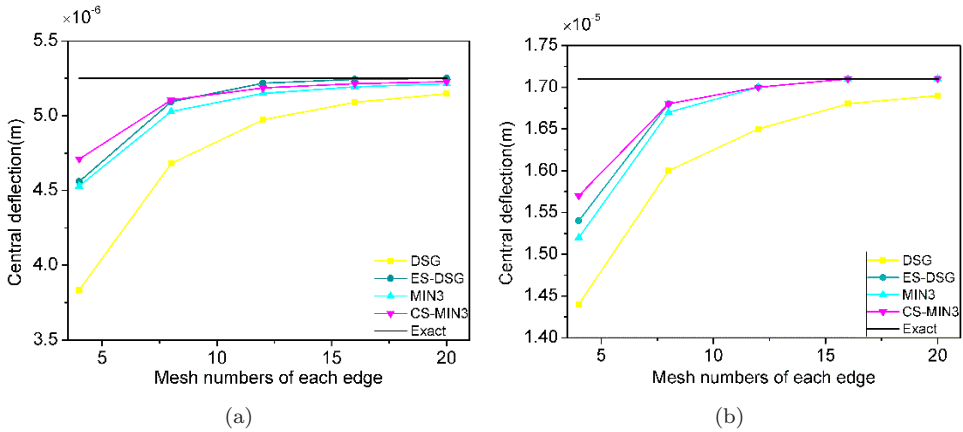
Fig. 7. Convergence curves of the rectangular plate with (a) clamped and (b) simply supported boundary conditions.

into five kinds of meshes $N \times N$ with the mesh number of each edge $N = 4, 8, 12, 16$ and 20 and Fig. 6(c) partly plots a quarter of the plate with these meshes. For comparison, the analytical solutions are calculated using the theoretical formulations of rectangular plate with uniform load.

Figure 7(a) clearly plots the convergence curves of the central deflection against different meshes $N \times N$ for clamped plate using four kinds of different elements, including the CS-MIN3, the MIN3, the DSG and the ES-DSG. It can be observed that with the same regular mesh, the CS-MIN3 performs better than DSG and MIN3, and even shows strong competition ability to ES-DSG. The convergence curve of the central deflection against different meshes $N \times N$ for simply supported plate is plotted in Fig. 7(b). Likewise, we can come to the same conclusions as drawn in the clamped boundary condition.

5.2. *Free vibration analysis for the uncoupled and coupled system*

5.2.1. *An cuboid acoustic cavity with a flexible plate on the top*

The geometrical parameters and material properties of the flexible plate considered in this part are the same as those of the rectangular plate described in the static analysis. The flexible plate is located on the top of a cuboid acoustic cavity which has the dimension of $0.44\,\mathrm{m} \times 0.38\,\mathrm{m} \times 0.48\,\mathrm{m}$ shown in Fig. 8. The boundary conditions on all edges of the plate are all simply supported with $w = 0$ and β_x, β_y are free at the edges. Except the cavity wall attached to the flexible plate, other five walls are supposed to be rigid. In our study, the flexible plate and the 3D cavity full of air ($\rho = 1.225\,\mathrm{kg/m}^3$ and $c = 340\,\mathrm{m/s}$) are modeled by triangular element and tetrahedron element, respectively.

The eigenfrequencies analysis for the uncoupled rectangular plate using CS-MIN3 and other three available elements are investigated first. 220 elements and
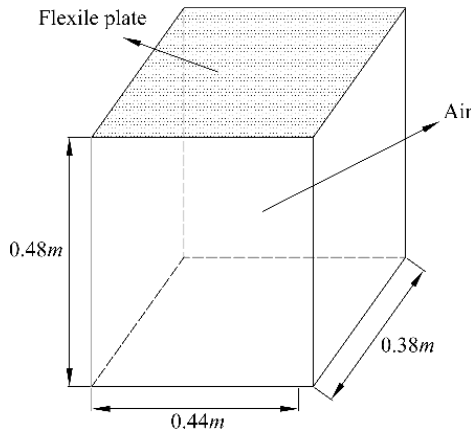
Fig. 8. A cuboid acoustic cavity with a flexible plate on the top.

Table 2. Eigenfrequencies of uncoupled plate obtained using the DSG, ES-DSG, MIN3 and CS-MIN3.

Modes	DSG (Hz)	ES-DSG (Hz)	MIN3 (Hz)	CS-MIN3 (Hz)	Reference (Hz)
1	30.51	29.90	30.11	29.78	29.46
2	72.43	70.03	70.83	69.63	67.19
3	86.52	83.64	84.90	83.50	80.06
4	134.02	127.06	128.85	124.99	117.67
5	150.09	141.30	144.50	140.69	130.07
6	189.58	180.16	184.43	179.88	164.39
7	215.73	202.18	206.30	198.21	180.35
8	249.81	229.72	237.57	225.72	201.80
9	268.60	249.64	258.90	249.61	218.10
10	324.15	302.21	310.03	296.51	264.15
11	355.33	330.67	342.88	319.08	268.11
12	374.40	333.87	344.54	329.81	282.44
13	432.38	391.05	407.11	380.86	319.57
14	444.33	407.69	428.93	407.12	331.28
15	460.33	423.86	437.16	411.99	351.45

132 nodes compose the 2D discretized domain. By using DSG, ES-DSG, MIN3 and CS-MIN3 with the same mesh, the first 15 nonrigid eigenfrequencies are obtained and listed in Table 2, together with the reference results computed using FEM with a very fine mesh. The eigenfrequencies of the 2D plate using the above four numerical methods are also plotted in Fig. 9(a). As shown in Table 2 and Fig. 9(a), the results obtained by the four numerical methods are all larger than the reference ones. When the mode order increases, the error becomes larger accordingly for all the four cases. It indicated that the stiffness of both the standard and smoothed FEM model is overly stiff. But for CS-MIN3, it can provide softer stiffness, and hence gives more accurate results than those using DSG and MIN3.
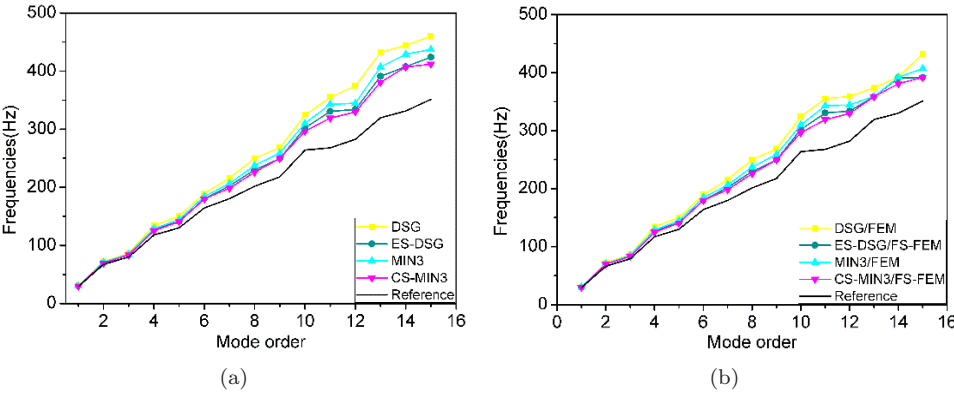
Fig. 9. Eigenfrequencies of the acoustic cavity system (a) uncoupled plate and (b) cavity coupled system.

Table 3. Eigenfrequencies of acoustic cavity obtained using the FEM and the FS-FEM.

Modes	FEM (Hz)	FS-FEM (Hz)	Reference (Hz)
1	358.87	358.62	357.29
2	392.26	391.76	389.77
3	454.81	454.26	451.32
4	534.78	533.26	528.75
5	583.04	581.34	575.62
6	605.26	603.21	596.33
7	708.46	705.18	695.17
8	728.08	725.58	714.58
9	797.14	794.56	779.55
10	834.90	830.32	813.97
11	869.04	863.49	845.17
12	880.81	876.13	857.52
13	930.30	924.64	900.76
14	930.88	926.51	902.63
15	962.70	955.01	930.72

For 3D acoustic cavity with rigid boundaries, both FEM and FS-FEM are implemented and the corresponding results are listed in Table 3. Compared with the references using FEM with fine mesh, the eigenfrequencies obtained using both FEM and FS-FEM are all larger than the reference results, and errors of both the two methods all increase with the increase of the frequencies. We can also find that the results obtained from FS-FEM are more accurate than those of FEM with the same mesh.

The above results obtained from both the 2D and 3D domains shed light on the effectiveness and accuracy of CS-FEM and FS-FEM. It is anticipated that the combination of CS-MIN3 and FS-FEM can probably perform very well and provide accurate results for the coupled systems. In the following part, the first 15 nonrigid

Table 4. Eigenfrequencies of cavity system obtained using the DSG/FEM, ES-DSG/FS-FEM, MIN3/FEM and the CS-MIN3/FS-FEM.

Modes	DSG/ FEM (Hz)	ES-DSG/ FS-FEM (Hz)	MIN3/ FEM (Hz)	CS-MIN3/ FS-FEM (Hz)	Reference (Hz)
1	30.50	29.89	30.10	29.77	29.45
2	72.41	70.00	70.81	69.61	66.16
3	86.49	83.61	84.87	83.46	79.10
4	133.98	127.01	128.82	124.95	116.87
5	150.04	141.25	144.45	140.64	130.02
6	189.51	180.08	184.37	179.80	164.03
7	215.66	202.10	206.23	198.13	179.59
8	249.72	229.62	237.49	225.62	201.06
9	268.53	249.56	258.84	249.53	217.48
10	324.04	302.09	309.92	296.39	263.85
11	354.95	330.46	342.67	318.96	267.78
12	359.04	333.74	344.43	329.61	281.73
13	374.25	358.53	358.85	358.46	319.16
14	392.30	390.88	392.27	380.83	330.03
15	432.22	391.83	406.99	391.76	351.11

eigenfrequencies are calculated through ES-FEM/FS-FEM model, CS-MIN3/FS-FEM model and FEM/FEM model (including the DSG/FEM and MIN3/FEM) and the results are listed in Table 4 and plotted in Fig. 9(b), including the references. The structure domain consisted of 220 triangular elements and the acoustic domain consisted of 4,503 tetrahedron elements. From the table and figure, we can find that all of these four coupled models can provide reliable results in low frequency range, but the results will gradually deviate from the references when the frequency increases. In comparison with FEM/FEM model, the proposed CS-MIN3/FS-FEM model could perform better and provide more exact results than other three coupled models. The reason is that both the 2D structure and 3D acoustic domains are smoothed by the smoothing operations. Therefore, the CS-MIN3/FS-MIN3 model is properly softer than the coupled FEM/FEM model and can provide more accurate eigenfrequencies prediction.

5.2.2. *Influence of mesh irregularity*

To investigate the influence of mesh irregularity for the standard FEM and S-FEM on solution accuracy, the plate of the above coupled acoustic cavity is meshed with regular and irregular nodes. In the discrete domain, the irregular mesh shapes are created by connecting two adjacent irregular nodes which are generated on the base of regularly distributed nodes. The irregular nodal coordinates can be obtained from the following formulations:

$$
\begin{aligned}
x_{ir} &= x_r + \Delta x_r * r_c * \beta_{ir}, \\
y_{ir} &= y_r + \Delta y_r * r_c * \beta_{ir},
\end{aligned}
\tag{51}
$$

where Δx_r and Δy_r represent the initial regular mesh sizes in x- and y-directions. r_c is a random number ranging from -1 to 1 which is generated by computer. β_{ir} is a prescribed irregularity degree which varies from 0 to 0.5. It is easy to find that a bigger value of β_{ir} will result in more irregular mesh shapes. Based on this, the flexible plate is discretized by using both regular mesh and irregular mesh which are presented in Fig. 10(a) regular mesh with irregularity parameter $\beta_{ir} = 0$; (b) irregular mesh with irregularity parameter $\beta_{ir} = 0.3$. The influence of mesh irregularity is described by the error defined as follows [He *et al.* (2009)]:

$$e = \frac{|f_{re} - f|}{f_{re}} \times 100\%,$$ (52)

where f_{re} and f are the reference result and the numerical result, respectively.

To illustrate the influence of mesh irregularity, the uncoupled plate is first investigated with the regular and irregular meshes consist of 220 triangular elements using the MIN3 and CS-MIN3 model. The first 10 nonrigid eigenfrequencies of the plate are given in Table 5, while the reference solution is also provided as above. And the corresponding errors are also listed in the table. The results showed that both MIN3 and CS-MIN3 results are deteriorated from the reference ones when irregular mesh is applied. But the CS-MIN3 performs better than MIN3 with the same number of nodes and elements, and the same irregularity parameter. These results indicate that even in very distorted mesh, the present CS-MIN3 can still work well.

In the following, the influence of the mesh irregularity to the coupled acoustic system is studied using the CS-MIN3/FS-FEM and MIN3/FEM models. The interaction surface between the air and plate consists of 220 triangular elements. Both the regular and irregular meshes of plate are shown in Fig. 10. By using the above two models, the first 10 nonrigid eigenfrequencies of the coupled system are listed in Table 6. From Table 6 it can be observed that the results of both MIN3/FEM model and CS-MIN3/FS-FEM model will deteriorate when the irregular meshes were employed. However, by comparing the errors using regular
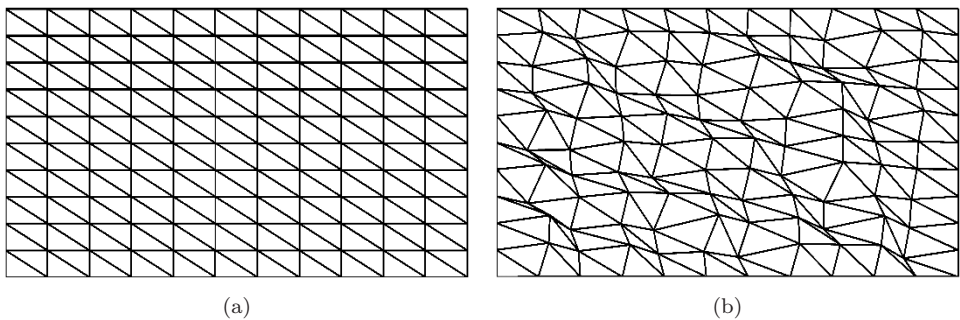

(a)   (b)

Fig. 10. The (a) regular and (b) irregular meshes generated with different nodal irregularity parameter.

Table 5. Eigenfrequencies of uncoupled plate obtained using MIN3 and CS-MIN3 with the regular and irregular mesh.

Modes	MIN3 (irr) (Hz)	Error (%)	MIN3 (re) (Hz)	Error (%)	CS-MIN3 (irr) (Hz)	Error (%)	CS-MIN3 (re) (Hz)	Error (%)	Reference (Hz)
1	30.26	2.73	30.11	2.21	29.91	1.54	29.78	1.11	29.46
2	71.71	6.73	70.83	5.42	70.30	4.63	69.63	3.64	67.19
3	86.15	7.61	84.90	6.05	84.43	5.46	83.50	4.30	80.06
4	131.29	11.58	128.85	9.51	126.73	7.70	124.99	6.22	117.67
5	148.03	13.81	144.50	11.09	143.15	10.06	140.69	8.17	130.07
6	189.52	15.29	184.43	12.20	183.55	11.66	179.88	9.42	164.39
7	212.95	18.07	206.30	14.39	202.79	12.44	198.21	9.90	180.35
8	243.92	20.87	237.57	17.73	230.52	14.23	225.72	11.85	201.80
9	268.20	22.97	258.90	18.71	255.60	17.20	249.61	14.45	218.10
10	326.01	23.42	310.03	17.37	308.54	16.80	296.51	12.25	264.15

Table 6. Eigenfrequencies of the cavity coupled system obtained using MIN3/FEM and CS-MIN3/FS-FEM with the regular and irregular mesh.

Modes	MIN3 /FEM (irr) (Hz)	Error (%)	MIN3 /FEM (re) (Hz)	Error (%)	CSMIN3 /FSFEM (irr) (Hz)	Error (%)	CSMIN3 /FSFEM (re) (Hz)	Error (%)	Reference (Hz)
1	30.26	2.73	30.11	2.21	29.91	1.54	29.78	1.11	29.46
2	71.71	6.73	70.83	5.42	70.30	4.63	69.63	3.64	67.19
3	86.15	7.61	84.90	6.05	84.43	5.46	83.50	4.30	80.06
4	131.29	11.58	128.85	9.51	126.73	7.70	124.99	6.22	117.67
5	148.03	13.81	144.50	11.09	143.15	10.06	140.69	8.17	130.07
6	189.52	15.29	184.43	12.20	183.55	11.66	179.88	9.42	164.39
7	212.95	18.07	206.30	14.39	202.79	12.44	198.21	9.90	180.35
8	243.92	20.87	237.57	17.73	230.52	14.23	225.72	11.85	201.80
9	268.20	22.97	258.90	18.71	255.60	17.20	249.61	14.45	218.10
10	326.01	23.42	310.03	17.37	308.54	16.80	296.51	12.25	264.15

and irregular meshes for both models, we can observe that the errors of smoothed coupled model change less than those of standard coupled model when the regular mesh is switched to irregular mesh. From the above descriptions, it indicates that the proposed CS-MIN3/FS-FEM model can give exact prediction of results for coupled system even using highly distorted meshes.

5.3. *Forced vibration analysis*

5.3.1. 3*D tube with a flexible plate at the end*

In this section, the model of 3D tube filled with air with a flexible circle plate at the right end is considered as shown in Fig. 11. The length of the tube is $l = 0.4\,\mathrm{m}$ and the diameter is $d = 0.2\,\mathrm{m}$. The circle plate is still made of aluminum with a thickness
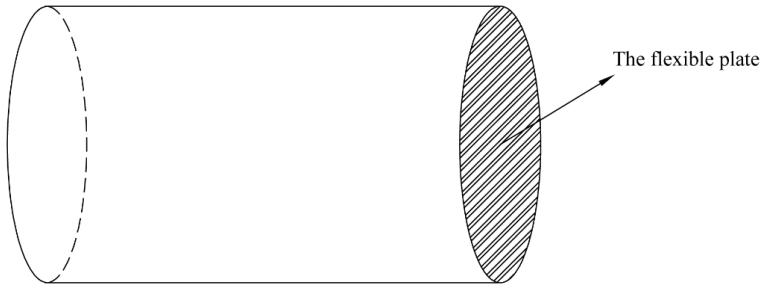
Fig. 11. The 3D tube filled with air with a flexible plate at the end.

of $t = 0.001\,\mathrm{m}$. Triangular elements and tetrahedron elements are employed to discretize the flexible plate and cylinder air cavity, respectively.

The uncoupled circle plate is first studied using MIN3 and CS-MIN3 with the same mesh which has 55 nodes and 84 elements. A harmonic uniform load with its amplitude $q = 1$ acts on the flexible plate that is simply supported. In our work, the center of the plate is chosen as the response point and the frequency range we adopted is from 1 to 1,000 Hz. The eigenfrequencies can be determined by picking the response peaks in the corresponding frequency range. Figure 12(a) plots the responses obtained using MIN3 and CS-MIN3 with the same numbers of nodes and elements. To make a comparison, the reference results are also presented in the figure, which are obtained by using FEM with a very fine mesh. As illustrated in Fig. 12(a), in lower frequency range, the results of both the MIN3 and CS-MIN3 agree well with the references, but when the frequencies increase, both accuracies of the two numerical methods decrease accordingly. However, compared with reference results, the CS-MIN3 can provide more accurate and closer
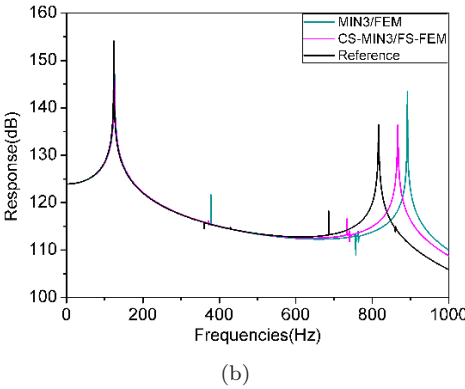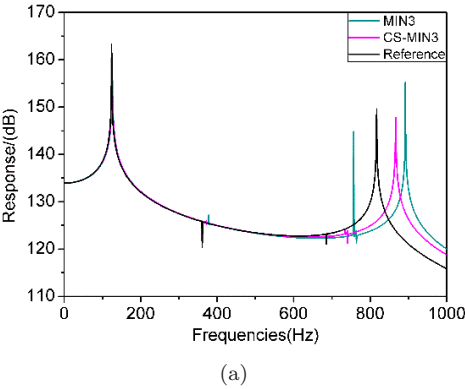

Fig. 12. Forced frequency response analysis using (a) MIN3 and CS-MIN3 for uncoupled plate and (b) MIN3/FEM and CS-MIN3/FS-FEM for the coupled plate.

solutions than MIN3. Through the cell-based smoothing operation, the stiffness of CS-MIN3 model is properly softened, and hence can well and truly predict the eigen-frequencies.

Next, the coupled circle plate attached with 3D cylinder acoustic cavity is considered and the present coupled MIN3/FEM and CS-MIN3/FS-FEM are implemented. Like the uncoupled plate, the same load and same response point are applicable for the couple plate which is still simply supported. The other five walls without the wall attached the plate are rigid. By using MIN3/FEM and CS-MIN3/FS-FEM, the harmonic responses of the center point of plate are plotted in the frequencies ranging from 1 to 1,000 Hz in Fig. 12(b). The figure demonstrates that the results of the coupled models are similar to those of uncoupled system. That is, in the lower frequency range, both the MIN3/FEM and CS-MIN3/FS-FEM can provide accurate results, but with the increase of frequencies, the results would become worse. Owing to coupled smoothing operations, including cell-based smoothing operation over the 2D plate and face-based operation over the 3D cylinder cavity, the coupled CS-MIN3/FS-FEM model can perform well not only in lower frequency range, but also in high frequency. So the smoothed coupled model can provide much better predictions for eigenfrequencies of coupled system.

5.3.2. *Automobile passenger compartment with flexible front panel*

For an automobile passenger compartment, the coupling effect between the flexible front panel and the compartment cavity cannot be ignored. In this section, a model of coupled passenger compartment system, as shown in Fig. 13, is adopted to investigate the performance of the coupled CS-MIN3/FS-FEM. The material of the front panel and the acoustic fluid are the same as the previous. The boundary conditions on all edges of the front panel are all clamped supported with $w = 0, \beta_x = 0$, and $\beta_y = 0$. A harmonic uniform load acts on the flexible front panel.
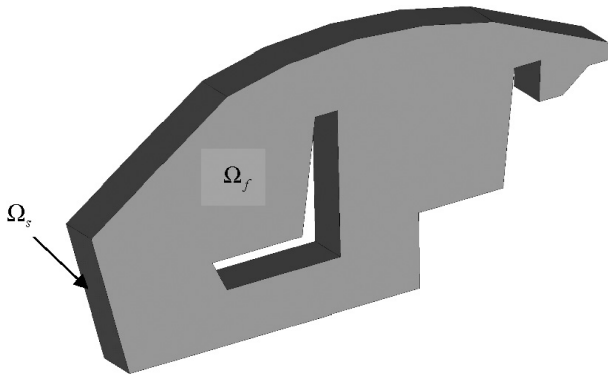

Fig. 13. The front panel Ω_s coupled with the acoustic cavity of passenger compartment Ω_f.
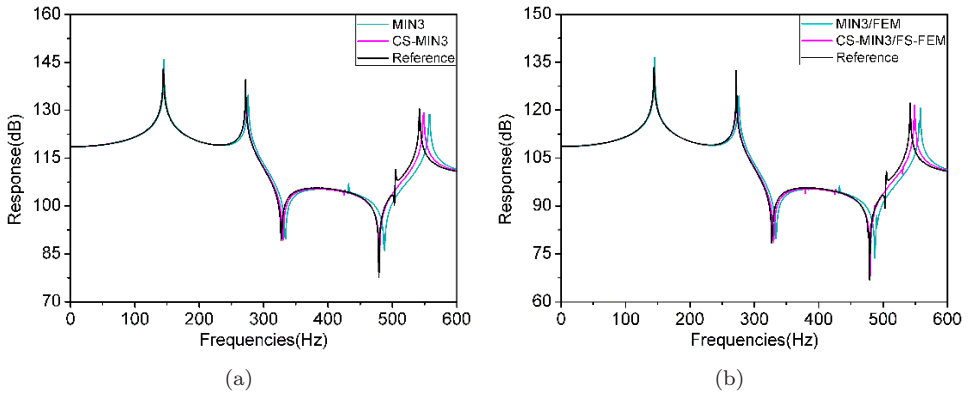
Fig. 14. Forced frequency response analysis using (a) MIN3 and CS-MIN3 for uncoupled plate and (b) MIN3/FEM and CS-MIN3/FS-FEM for the coupled panel.

The center of the front panel is chosen as the response point and the frequency range is from 1 to 600 Hz. Figures 14(a) and 14(b) plots the responses of the uncoupled and coupled panel, respectively. The pictures show that for both the uncoupled and coupled panel, the results are all in good agreement with the reference ones at low frequency. With the increase of frequency, it can be found that in the uncoupled system, the CS-MIN3 performs better than MIN3, while the CS-MIN3/FS-FEM can provide more accurate solutions than MIN3/FEM in the coupled system. It again conformed the obtained comments as in the above 3D Tube with a Flexible Plate.

6. Conclusions

In this work, the proposed CS-FEM-MIN3/FS-FEM method is employed to solve the structural–acoustic problems of a plate interacted with 3D fluid medium. As both CS-FEM and FS-FEM are based on linear equations, this coupled method is only effective to solve linear problems. The discretized system equations are formulated by using the smoothed Galerkin weak form. Through the formulations and numerical examples, we can draw some concluding remarks as follows:

(1) The CS-MIN3 is formulated by interoperating the cell-based smoothed strain technique with the original MIN3, and meanwhile, $Gkt^3/(t^2 + \alpha h_e^2)$ is adopted as the transverse shear stiffness constitutive coefficient $\hat{\mathbf{D}}_s$. Hence, the CS-MIN3 can avoid shear locking problem and provide high-accuracy solutions for the plate analysis.
(2) For static analysis, the results of the CS-MIN3 are in good agreement with the exact solutions and results of other three numerical methods in this paper. The CS-MIN3 shows higher rate of convergence and is much more accurate than DSG, MIN3 and is also a good competitor to ES-DSG.
(3) For dynamic analysis (including free and forced vibration analyses), the CS-MIN3 is temporally stable, agrees well with the reference results and show

some superior properties. The CS-MIN3 gives much more accurate results than the DSG, MIN3, and is a good competitor to ES-DSG.

(4) The CS-MIN3 is less sensitive to the mesh irregularity and it can give acceptable solution even with extremely irregular mesh, while the FEM-MIN3, however, is sensitive to the quality of meshes.

(5) The coupled CS-FEM-MIN3/FS-FEM can be implemented directly with the same degrees of freedom compared with the standard coupled FEM/FEM which is easy to use for the coupled structural–acoustic problems. Compared with the standard coupled FEM/FEM, the coupled CS-FEM-MIN3/FS-FEM can achieve more accurate solutions owing to the properly softening effects through the cell-based/face-based gradient smoothing operations.

(6) The coupled CS-FEM-MIN3/FS-FEM performs very well with triangular and tetrahedron meshes which are simple and easy in automatic meshing. Hence, it is more likely to give accurate prediction of the engineering practice problems which are often of complicated geometries.

References

Alvarez, G. B., Loula, A. F. D., do Carmo, E. G. D. and Rochinha, F. A. [2006] "A discontinuous finite element formulation for Helmholtz equation," *Comput. Methods Appl. Mech. Eng.* **195**, 4018–4035.

Bathe, K. J., Nitikitpaiboon, C. and Wang, X. [1995] "A mixed displacement-based finite element formulation for acoustic fluid-structure interaction," *Comput. Struct.* **56**, 225–237.

Bischoff, M. and Bletzinger, K. U. [2001] "Stabilized DSG plate and shell elements," in *Trends in Computational Structural Mechanics* (CIMNE, Barcelona, Spain), pp. 253–263.

Bouillard, P. and Suleaub, S. [1998] "Element-Free Galerkin solutions for Helmholtz problems: Formulation and numerical assessment of the pollution effect," *Comput. Methods Appl. Mech. Eng.* **162**, 317–335.

Cheng, H., Chen, J., Zhang, Y., Bi, C. and Gao, Y. [2009] "A multi-domain boundary element formulation for acoustic frequency sensitivity analysis," *Eng. Anal. Bound. Elem.* **33**, 815–821.

Cheng, L., White, R. D. and Grosh, K. [2008] "Three-dimensional viscous finite element formulation for acoustic fluid–structure interaction," *Comput. Methods Appl. Mech. Eng.* **197**, 4160–4172.

Citarella, R., Federico, L. and Cicatiello, A. [2007] "Modal acoustic transfer vector approach in a FEM–BEM vibro–acoustic analysis," *Eng. Anal. Bound. Elem.* **31**, 248–258.

Everstine, G. C. [1981] "A symmetric potential formulation for fluid–structure interaction," *J. Sound Vib.* **79**, 157–160.

Harari, I. and Hughes, T. J. [1992] "Galerkin/least-squares finite element methods for the reduced wave equation with non-reflecting boundary conditions in unbounded domains," *Comput. Methods Appl. Mech. Eng.* **98**, 411–454.

He, Z. C., Liu, G. R., Zhong, Z. H., Cui, X. Y., Zhang, G. Y. and Cheng, A. G. [2010a] "A coupled edge-/face-based smoothed finite element method for structural–acoustic problems," *Appl. Acoust.* **71**, 955–964.

He, Z. C., Liu, G. R., Zhong, Z. H., Wu, S. C., Zhang, G. Y. and Cheng, A. G. [2009] "An edge-based smoothed finite element method (ES-FEM) for analyzing three-dimensional acoustic problems," *Comput. Methods Appl. Mech. Eng.* **199**, 20–33.

He, Z. C., Liu, G. R., Zhong, Z. H., Zhang, G. Y. and Cheng, A. G. [2010b] "Coupled analysis of 3D structural–acoustic problems using the edge-based smoothed finite element method/finite element method," *Finite Elem. Anal. Des.* **46**, 1114–1121.

He, Z. C., Liu, G. R., Zhong, Z. H., Zhang, G. Y. and Cheng, A. G. [2011] "A coupled ES-FEM/BEM method for fluid–structure interaction problems," *Eng. Anal. Bound. Elem.* **35**, 140–147.

Li, W., Chai, Y., Lei, M. and Liu, G. R. [2014] "Analysis of coupled structural–acoustic problems based on the smoothed finite element method (S-FEM)," *Eng. Anal. Bound. Elem.* **42**, 84–91.

Liu, G. R. [2008] "A generalized gradient smoothing technique and the smoothed bilinear form for Galerkin formulation of a wide class of computational methods," *Int. J. Comput. Methods* **5**, 199–236.

Liu, G. R. and Gu, Y. T. [2001] "A point interpolation method for two-dimensional solids," *Int. J. Numer. Methods Eng.* **50**, 937–951.

Liu, G. R., Dai, K. Y. and Nguyen, T. T. [2007a] "A smoothed finite element method for mechanics problems," *Comput. Mech.* **39**, 859–877.

Liu, G. R., Nguyen, T. T., Dai, K. Y. and Lam, K. Y. [2007b] "Theoretical aspects of the smoothed finite element method (SFEM)," *Int. J. Numer. Methods Eng.* **71**, 902–930.

Liu, G. R., Nguyen-Thoi, T. and Lam, K. Y. [2009] "An edge-based smoothed finite element method (ES-FEM) for static, free and forced vibration analyses of solids," *J. Sound Vib.* **320**, 1100–1130.

Liu, G. R. and Quek, S. S. [2003] *Finite Element Method*: *A Practical Course* (Butterworth-Heinemann, Burlington, MA, USA).

Liu, G. R., Zhang, G. Y., Dai, K. Y., Wang, Y. Y., Zhong, Z. H., Li, G. Y. and Han, X. [2005] "A linearly conforming point interpolation method (LC-PIM) for 2D solid mechanics problems," *Int. J. Comput. Methods* **2**, 645–665.

Loula, A. F., Alvarez, G. B., do Carmo, E. G. and Rochinha, F. A. [2007] "A discontinuous finite element method at element level for Helmholtz equation," *Comput. Methods Appl. Mech. Eng.* **196**, 867–878.

Luong-Van, H., Nguyen-Thoi, T., Liu, G. R. and Phung-Van, P. [2014] "A cell-based smoothed finite element method using three-node shear-locking free Mindlin plate element (CS-FEM-MIN3) for dynamic response of laminated composite plates on viscoelastic foundation," *Eng. Anal. Bound. Elem.* **42**, 8–19.

Lyly, M., Stenberg, R. and Vihinen, T. [1993] "A stable bilinear element for the Reissner-Mindlin plate model," *Comput. Meth. Appl. Mech. Eng.* **110**, 343–357.

Mukherjee, S. and Liu, Y. [2013] "The boundary element method," *Int. J. Comput. Methods*, **10**, 1350037-1–91.

Nguyen-Thoi, T., Liu, G. R., Lam, K. Y. and Zhang, G. Y. [2009a] "A face-based smoothed finite element method (FS-FEM) for 3D linear and geometrically non-linear solid mechanics problems using 4-node tetrahedral elements," *Int. J. Numer. Methods Eng.* **78**, 324–353.

Nguyen-Thoi, T., Liu, G. R., Vu-Do, H. C. and Nguyen-Xuan, H. [2009b] "A face-based smoothed finite element method (FS-FEM) for visco-elastoplastic analyses of 3D solids using tetrahedral mesh," *Comput. Meth. Appl. Mech. Eng.* **198**, 3479–3498.

Nguyen-Thoi, T., Phung-Van, P., Luong-Van, H., Nguyen-Van, H. and Nguyen-Xuan, H. [2013a] "A cell-based smoothed three-node Mindlin plate element (CS-MIN3) for static and free vibration analyses of plates," *Comput. Mech.* **51**, 65–81.

Nguyen-Thoi, T., Phung-Van, P., Rabczuk, T., Nguyen-Xuan, H. and Le-Van, C. [2013b] "An application of the ES-FEM in solid domain for dynamic analysis of 2D fluid–solid interaction problems," *Int. J Comput. Methods* **10**, 1340003-1–28.

Tessler, A. and Hughes, T. J. R. [1985] "A three-node Mindlin plate element with improved transverse shear," *Comput. Meth. Appl. Mech. Eng.* **50**, 71–101.

Thompson, L. L. and Pinsky, P. M. [1995] "A Galerkin least-squares finite element method for the two-dimensional Helmholtz equation," *Int. J. Numer. Methods Eng.* **38**, 371–397.

Wang, X. and Bathe, K. J. [1997] "Displacement/pressure based mixed finite element formulations for acoustic fluid–structure interaction problems," *Int. J. Numer. Methods Eng.* **40**, 2001–2017.

Zhang, G. Y., Liu, G. R., Wang, Y. Y., Huang, H. T., Zhong, Z. H., Li, G. Y. and Han, X. [2007] "A linearly conforming point interpolation method (LC-PIM) for three-dimensional elasticity problems," *Int. J. Numer. Methods Eng.* **72**, 1524–1543.

Zienkiewicz, O. C. and Bettess, P. [1978] "Fluid–structure dynamic interaction and wave forces: An introduction to numerical treatment," *Int. J. Numer. Methods Eng.* **13**, 1–16.